Magnetic field control of the Franck-Condon coupling of few-electron quantum states

P. L. Stiller, A. Dirnaichner, D. R. Schmid, and A. K. Hüttel*
Institute for Experimental and Applied Physics, University of Regensburg, 93040 Regensburg, Germany
(Dated: December 6, 2018)

Suspended carbon nanotubes display at cryogenic temperatures a distinct interaction between the quantized longitudinal vibration of the macromolecule and its embedded quantum dot. We present data on such Franck-Condon side bands at known absolute number $N_{\mathrm{el}} = 1$ and $N_{\mathrm{el}} = 2$ of conduction band electrons and consequently well-defined electronic ground and excited states in a clean nanotube device. The side bands evolve only at a large axial magnetic field and display a distinct magnetic field dependence of the Franck-Condon coupling, different for different electronic base states and indicating a valley-dependent electron-vibron coupling. A tentative model for this effect is discussed.

Vibrational degrees of freedom, typically approximated at small deflection as harmonic oscillators, contribute in many ways to the fundamental properties of matter. The Franck-Condon principle [1, 2] relates vibrational wave functions in molecular physics to the intensity envelope of vibrational side bands in optical spectra. This principle, where an electronic transition is assumed to be instantaneous compared to the slow motion of the nuclei, also becomes directly visible in electronic low-temperature transport spectroscopy of single (macro)molecules [3–12]. An experimental system where such Franck-Condon sidebands have been observed consistently is the longitudinal (stretching mode) vibration of a suspended single wall carbon nanotube (SW-CNT) quantum dot [9, 13–19]. Results range from the nanotube length dependence of the vibration frequency [9], or thermal occupation of a vibration mode [14], all the way to electronic pumping of nonequilibrium occupation [15], spin-vibron coupling [17] and a spin-dependent, electrostatically tunable electron-vibron coupling [19].

In this Letter, we present first observations of Franck-Condon sidebands at known absolute number $N_{\mathrm{el}} = 1$ and $N_{\mathrm{el}} = 2$ of conduction band electrons in the unperturbed carbon nanotube transport spectrum. The vibrational sidebands evolve only at large axial magnetic field B. The resulting millikelvin transport spectrum displays different sideband behaviour depending on the electronic base state; the data indicates a valley-dependent Franck-Condon electron-vibron coupling parameter [4]. A tentative model for the observed phenomenon is discussed.

A sketch of the measured device is depicted in Fig. 1(a). Following [20], a carbon nanotube is grown over pre-defined rhenium contact electrodes and etched trenches. Subsequently the device is cooled down in a dilution refrigerator and characterized electronically at a base temperature of $T_{\mathrm{mc}} \leq 25\,\mathrm{mK}$, immersed into the diluted phase of the ^{3}He/^{4}He mixture. The length of the suspended nanotube segment is $L = 700\,\mathrm{nm}$. As can be seen in the current trace at low bias of Fig. 1(b), the device displays the behaviour of a small bandgap nanotube, with transparent hole conduction and strong Coulomb blockade at low electron numbers. The first Coulomb oscillations display very low current and require particular care to be resolved, see Fig. 1(c). Here, the opaque tunnel barriers are given by p-n junctions extended along the nanotube, between the electrostatically induced n-quantum dot and p-behaviour near the leads [21, 22].

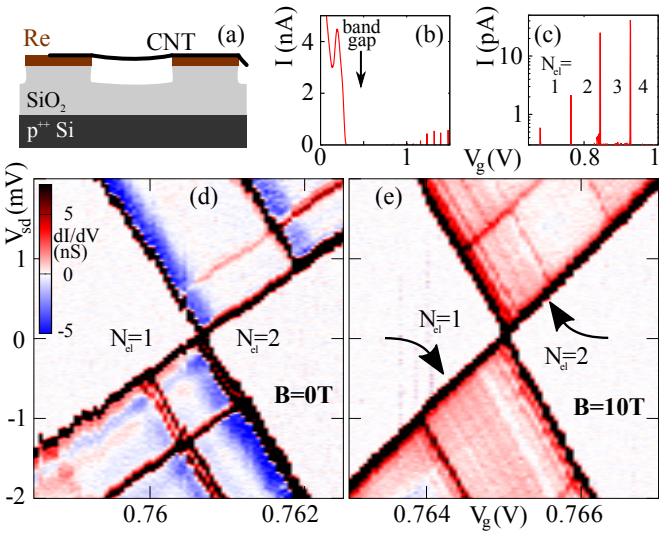

FIG. 1. (a) Schematic device geometry. A carbon nanotube is grown in situ across pre-defined rhenium contact electrodes and a trench. (b) Overview device characterization $I(V_{\mathrm{g}})$ at $V_{\mathrm{sd}} = 50\,\mu\mathrm{V}$, showing transparent behaviour in hole conduction, the band gap, and Coulomb oscillations in electron conduction. (c) Coulomb oscillations $I(V_{\mathrm{g}})$ for $V_{\mathrm{sd}} = 0.5\,\mathrm{mV}$ near the electronic band gap, with absolute electron numbers N_{el} marked. (d,e) Differential conductance $\mathrm{d}I/\mathrm{d}V_{\mathrm{sd}}$ at the $1 \leq N_{\mathrm{el}} \leq 2$ transition, for a magnetic field of (d) $B = 0$ and (e) $B = 10\,\mathrm{T}$ parallel to the carbon nanotube axis (identical color scale, cut off at +7 nS for better contrast).

In the following we focus on the $1 \leq N_{\mathrm{el}} \leq 2$ transition, i.e., the second Coulomb oscillation of conductance at the electron side of the band gap. Fig. 1(d) and Fig. 1(e) display the stability diagram around the corresponding degeneracy point, for (d) $B = 0$ and for (e) a magnetic field $B = 10\,\mathrm{T}$ applied in parallel to the carbon nanotube axis. The overall conductance is very low; even so, the color scale in the figure has been cut off such as to fo-

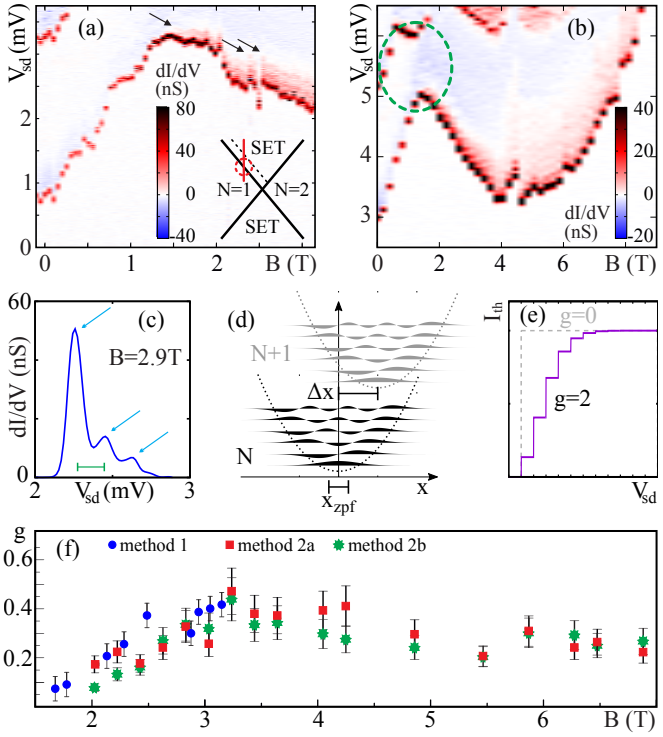

FIG. 2. (a) Differential conductance as function of magnetic field parallel to the nanotube axis B and bias voltage $V_{\rm sd}$, $\mathrm{d}I/\mathrm{d}V_{\rm sd}(B, V_{\rm sd})$, at constant $V_{\rm g} = 0.7599\,\mathrm{V}$. This cuts through the $1 \leq N_{\rm el} \leq 2$ single electron tunneling region, as sketched in the inset. (b) Similar measurement of $\mathrm{d}I/\mathrm{d}V_{\rm sd}(B, V_{\rm sd})$, covering a larger magnetic field range at lower resolution; $V_{\rm g} = 0.758\,\mathrm{V}$. (c) Line trace $\mathrm{d}I/\mathrm{d}V_{\rm sd}(V_{\rm sd})$ from (a) at $B = 2.9\,\mathrm{T}$, clearly displaying the edge of the Coulom blockade region, corresponding to the $1 \leq N_{\rm el} \leq 2$ ground state transition, and several conductance side peaks. (d) Illustration of the Franck-Condon coupling mechanism, see the text. (e) Schematic drawing of the stepwise current $I_{\rm th}(V_{\rm sd})$ increase at increasing bias voltage due to Franck-Condon coupling, here for $\Delta x = 2x_{\rm zpf}$ and thus $g = 2$ as in (d). (f) Experimentally obtained Franck-Condon coupling parameter $g(B)$ as function of the magnetic field; the different point types stand for different evaulation methods, see the Supplemental Material [23] for details.

cus on the substructure of the single electron tunneling (SET) regions. The strong black lines, corresponding to electronic excitations, shift with magnetic field; their detailed behaviour, as well as the negative differential conductance at $B = 0$, is topic of ongoing analysis and will be presented in a future publication. The figures display a clear qualitative difference between $B = 0$, Fig. 1(d), and $B = 10\,\mathrm{T}$, Fig. 1(e): while the areas between the electronic excitation lines are featureless in Fig. 1(d), in Fig. 1(e) they display a multitude of fine, closely spaced conductance resonances (see the arrows in Fig. 1(e)).

The plot of Fig. 2(a) demonstrates the emergence of this phenomenon. Here, we show the differential conductance $\mathrm{d}I/\mathrm{d}V_{\rm sd}(B, V_{\rm sd})$ as function of an applied magnetic field B parallel to the carbon nanotube axis and of the bias voltage $V_{\rm sd}$. The gate voltage is kept constant and chosen such that we trace across the $N_{\rm el} = 1$ edge of the $1 \leq N_{\rm el} \leq 2$ single electron tunneling region, see the inset of Fig. 2(a) for a sketch.

For $B = 0$, the SET region edge, visible as line of differential conductance, is located at approximately $V_{\rm sd} = 0.8\,\mathrm{mV}$. Due to a shift in energy of the electronic states involved in transport, it rapidly moves to higher bias voltages until $B \simeq 1.5\,\mathrm{T}$ is reached. Here, the magnetic field induces a change in ground state, leading to a different energy dispersion. Soon afterwards, side bands of the differential conductance line emerge, see the arrows in Fig. 2(a). Figure 2(b) displays a larger parameter range than Fig. 2(a), though measured at reduced resolution. Still, the side bands of the conductance line become clearly visible as an asymmetric broadening of the main conductance line (towards higher bias voltages).

An example trace cut from Fig. 2(a) is shown in Fig. 2(c). An analysis of the relative peak positions in each such recorded trace $I(V_{\rm sd})$ is given in the Supplemental Material [23]. Its conclusion is that the side bands are equidistant within each trace, and that the corresponding excitation energy is magnetic field independent and given by $\Delta\epsilon \simeq 60\,\mu\mathrm{eV}$. This strongly indicates a harmonic oscillator independent of the electronic spectrum. Given its energy scale, we can identify it with the longitudinal, stretching mode vibration of the carbon nanotube [9].

In multiple publications, the mechanism leading to vibrational side bands in transport spectroscopy has been identified as the Franck-Condon principle [4, 7, 9]. As sketched in Fig. 2(d), the equilibrium position of the vibrational harmonic oscillator depends on the number of charges $N_{\rm el}$ on the nanotube; the rate of single electron tunneling through its quantum dot is modified by the spatial overlap of the involved harmonic oscillator states $|\langle\Psi_m(N)\,|\,\Psi_n(N+1)\rangle|^2 = |\langle\Psi_m(x)\,|\,\Psi_n(x+\Delta x)\rangle|^2$, with m and n as the vibrational occupation quantum number at N and $N+1$ electrons, respectively. Δx is the displacement of the harmonic oscillator by the additional charge, cf. Fig. 2(d). The coupling strength is parametrized via the Franck-Condon coupling parameter $g = (\Delta x/x_{\rm zpf})^2/2$, comparing Δx with the characteristic length scale of the harmonic oscillator $x_{\rm zpf} = \sqrt{\hbar/m\omega}$.

As sketched in Fig. 2(e), a finite value of g corresponds to a specific redistribution of current between vibrational channels: the current at the bias voltage corresponding to the bare electronic transition energy $N \longrightarrow N+1$ decreases, but additional steps of current emerge whenever an additional vibration state becomes energetically available. g can be calculated from the current step or differential conductance peak height ratios. A more detailed discussion of this model and its application here can be found in the Supplemental Material [23].

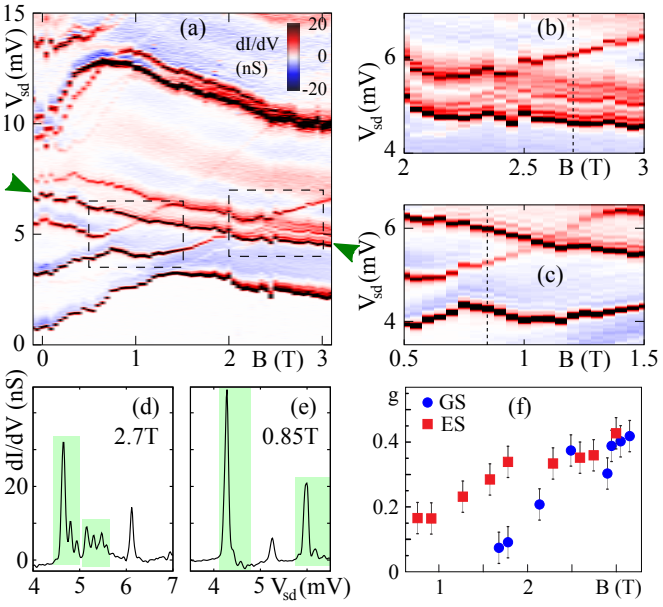

FIG. 3. (a) Two-electron excitation spectrum: Differential conductance $\mathrm{d}I/\mathrm{d}V_{\mathrm{sd}}(B, V_{\mathrm{sd}})$ as function of magnetic field B and bias voltage V_{sd}, for constant gate voltage $V_{\mathrm{g}} = 0.7599\,\mathrm{V}$. (b), (c) Detail enlargements (same color scale) of the areas marked with dashed rectangles in (a). (d), (e) Trace cuts $\mathrm{d}I/\mathrm{d}V_{\mathrm{sd}}(V_{\mathrm{sd}})$ at the positions indicated in (b) and (c). Conductance peaks with clear vibrational side bands are shaded. (f) Magnetic field evolution of the Franck-Condon coupling $g(B)$ for the excited state transition marked with arrowheads in (a) (red squares), compared with the ground state transition (blue dots, same data as in Fig. 2(f)).

The result of this evaluation for each trace $I(V_{\mathrm{sd}})$ or $\mathrm{d}I/\mathrm{d}V_{\mathrm{sd}}(V_{\mathrm{sd}})$ at fixed B is plotted in Fig. 2(f). It shows the resulting magnetic field dependence of the Franck-Condon coupling parameter $g(B)$ for the $N_{\mathrm{el}} = 1 \longrightarrow N_{\mathrm{el}} = 2$ ground state transition. The absence of side bands for $B < 1.5\,\mathrm{T}$ corresponds to an absence of coupling, i.e., $g \sim 0$. For $B \geq 1.5\,\mathrm{T}$ the coupling increases monotonously, reaching a maximum value $g(B) = 0.4$ at $B = 3\,\mathrm{T}$. Subsequently, we observe a slow decrease.

To our best knowledge, no similar observations of a magnetic field dependent electron-vibron coupling have been published so far. Its onset at an anticrossing of electronic states, see the dashed ellipsoid in Fig. 2(b), suggests a connection to the precise electronic quantum numbers. As opposed to previous reports on the longitudinal vibration mode [9, 13–15, 17, 19], here we are characterizing a device where the nanotube has grown cleanly across pre-existing contacts, and no (accidental or intentional) strongly inhomogeneuous potential should distort the wave functions in the suspended macromolecule away from the metallic contacts. With this in mind, we have analyzed the vibrational side band behaviour of the electronic *excited* states in the transport spectrum.

A plot of the differential conductance at fixed gate voltage, as function of B and the bias voltage V_{sd}, now over a large bias range, is shown in Fig. 3(a). A preliminary evaluation of the data of Fig. 3(a), taking also into account the one-electron excitation spectrum of the device [24], reveals two energetically close shells with both intra- and inter-shell exchange interaction; detailed modelling of the two electron transport spectrum will be the topic of a separate work [25]. Here, we limit ourselves to a straightforward classification of conductance lines by magnetic field dispersion. Since the dominant magnetic field dependence in an axial field originates in the electronic orbital momentum μ_{orb}, see, e.g., [24, 26, 27], both one- and two-electron quantum states become at large field orbital momentum eigenstates, and the slope of a line in the figure indicates the momentum *change* when a second electron tunnels onto the quantum dot, proportional to $\mathrm{d}(\Delta E(B))/\mathrm{d}B = \mathrm{d}(E_2(B) - E_1(B))/\mathrm{d}B$. Assuming arbitrary combinations of one- and two-electron states with energies $E_1(B)$ and $E_2(B)$, this allows for slopes $\mathrm{d}(\Delta E)/\mathrm{d}B \approx n\mu_{\mathrm{orb}}B$, $n \in \{-3, -1, 1, 3\}$; if the momentum of the first electron remains unchanged, only $n \in \{-1, 1\}$ remains possible. From this we can classify the conductance lines of Fig. 3(a). In the low-bias region of the figure, two dominant slopes clearly emerge; we identify these with the addition of a K'-valley electron (downward slope) or a K-valley electron (upward slope), respectively [24, 26, 27].

Figures 3(b) and 3(c) enlarge the regions marked in 3(a) with dashed rectangles. As for the ground state resonance, also here, the harmonic side bands are immediately visible. However, not all electronic states display the same behaviour; at a glance, only the down-sloping spectral lines, where an electron is added in a K'-valley state, exhibit electron-vibron coupling. Also the trace cuts at $B = 2.70\,\mathrm{T}$ (Fig. 3(d)) and $B = 0.85\,\mathrm{T}$ (Fig. 3(e)) demonstrate this clearly, with the resonances accompanied by sidebands highlighted in green. We have performed an analysis of the electronic states in Fig. 3(a), by dividing them into segments at each crossing or anticrossing and checking each segment for vibrational sidebands. The result is provided in the Supplemental Material [23]. While it is not always possible to decide unambiguously whether vibrational sidebands are present, the results support the hypothesis of valley dependent coupling.

Extracting the Franck-Condon coupling parameter for an exemplary excited state transition (green arrowheads in Fig. 3(a)), we compare its evolution over the entire field range $0.5\,\mathrm{T} \lesssim B \lesssim 3.5\,\mathrm{T}$ with the two-electron ground state transition in Fig. 3(f). A finite g persists to much lower magnetic field for the excited state transition; linear interpolation to $B = 0$ results in $g(0) \leq 0.15$. The faster onset of coupling for the ground state transition is consistent with valley dependence and the change in ground state quantum numbers at $B \simeq 1.5\,\mathrm{T}$, see the

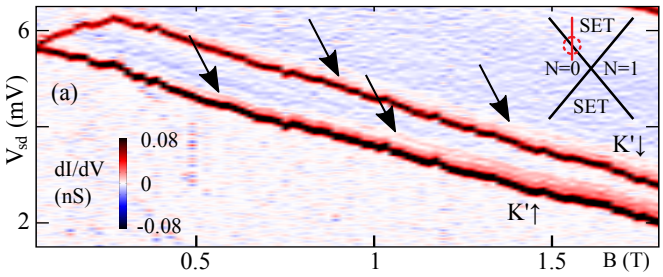

FIG. 4. High magnetic field behaviour of the $0 \leq N_{\mathrm{el}} \leq 1$ one electron ground state transition. Traces of vibrational side bands are indicated by arrows. Note that the color scale is cut off at ± 0.08 nS.

structure marked with a dashed ellipsoid in Fig. 2(b).

It remains to clarify whether the observed effect is specific to the absolute electron number $1 \leq N_{\mathrm{el}} \leq 2$ region. Figure 4 displays the magnetic field dependence of a cut across the $0 \leq N_{\mathrm{el}} \leq 1$ ground state transtion. Indeed, also here where an electron tunnels into a $|K'\rangle$ state of the otherwise unoccupied conduction band, an onset of harmonic side bands can be identified, for both spin alignments. Given the significantly lower conductance here, see the color bar in Fig. 4, a more detailed evaluation turns out to be challenging. We can however conclude that the electron-vibron coupling is already inherent to single electron phenomena, and not limited to two-electron states [19]. This indicates a selectivity directly related to the single-particle valley quantum number.

In published literature, Weber *et al.* [19] have reported on an electronic state dependent Franck-Condon coupling in a $N_{\mathrm{el}} = 4n+2$ quantum dot, switchable via a local gate potential deformation. They apply a magnetic field perpendicular to the nanotube, and see no effect of that field on the vibrational side bands. Due to valley mixing and the field direction, their data is in the regime of bonding and antibonding valley linear combinations. A different electron-vibron coupling of (valley-ground state) spin singlet and (valley-distributed) spin triplet states, as observed in [19], obviously can indicate a valley-dependent effect. Whether this can be related to the results reported here however requires further analysis.

Models discussing strong electron-vibron coupling $g \sim 1$ in carbon nanotube quantum dots typically assume an inhomogeneuous charge distribution along the macromolecule relative to the vibration mode envelope, or more generally, a different localization of electron and vibron wave function, see, e.g., [9, 28–30]. This is consistent with the occurrence of Franck-Condon side bands in devices with localized gates close to the nanotube [14, 18, 19]. In previous devices without such an electrode, a local potential may have been introduced via fabrication defects or impurities on the nanotube [9, 13, 15]. These expanations do not lend themselves for the device presented here, displaying a highly regular one electron spectrum [24] and a regular addition spectrum over a large electron number range [31]. Nevertheless, the formation of the quantum dot via gate-induced p-n junctions, see, e.g., [21, 22], leads in the low electron number limit to an electronic confinement much more narrow than the mechanically active device length, and centered within the suspended nanotube segment.

Comparison with [19, 28, 30] then suggests that the axial magnetic field modifies the Franck-Condon coupling g by shifting the electronic wave function relative to the vibron. A mechanism which may have this effect was recently proposed in [24], based on [32–34]: essentially, the axial magnetic field introduces a valley-dependent Aharonov-Bohm phase, modifying the longitudinal boundary conditions and thereby also the longitudinal profile of the electronic wave function. Modelling will have to take into account the bipartite structure of the nanotube lattice to verify the impact of this on the coupling parameter.

Finally, an interesting detail of our measurement is that the transport spectra were measured with the carbon nanotube immersed into the ^{3}He/^{4}He mixture (D phase) of the dilution refrigerator. Its viscosity at base temperature, $\eta \sim 10^{-5}$ N s/m^2 [35], is sufficiently high to mechanically dampen the transversal vibration mode [36]. As observed here, this does not affect the longitudinal mode; a likely explanation is that motion along the nanotube axis does not require displacement of liquid.

In conclusion, we demonstrate that vibrational sidebands emerge in the $0 \leq N_{\mathrm{el}} \leq 2$ transport spectrum of an ultraclean nanotube at a finite magnetic field parallel to the nanotube axis. The sidebands are equidistant, with a field-independent oscillator quantum. Relative peak intensities are consistent with Franck-Condon theory [4]; their evaluation results in a field-dependent coupling constant $g(B)$. Our data indicate that only conductance lines corresponding to the addition of a K' valley electron develop a finite coupling parameter g. A tentative mechanism for this can be a field-induced and valley-selective modification of the electronic wavefunction envelope [24].

We would like to thank M. Margańska, M. Grifoni, A. Donarini, Ch. Strunk, and E. A. Laird for insightful discussions, and Ch. Strunk and D. Weiss for the use of experimental facilities. The data has been recorded using the Lab::Measurement software package [37]. The authors acknowledge financial support by the Deutsche Forschungsgemeinschaft (Emmy Noether grant Hu 1808/1, GRK 1570, SFB 689, SFB 1277) and by the Studienstiftung des deutschen Volkes.

* andreas.huettel@ur.de

[1] J. Franck, "Elementary processes of photochemical reactions," Trans. Faraday Soc. **21**, 536 (1926).

[2] E. Condon, "A theory of intensity distribution in band systems," Phys. Rev. **28**, 1182 (1926).

[3] H. Park, J. Park, A. K. L. Lim, E. H. Anderson, A. P. Alivisatos, and P. L. McEuen, "Nanomechanical oscillations in a single-C60 transistor," Nature **407**, 57 (2000).

[4] S. Braig and K. Flensberg, "Vibrational sidebands and dissipative tunneling in molecular transistors," Phys. Rev. B **68**, 205324 (2003).

[5] B. J. LeRoy, S. G. Lemay, J. Kong, and C. Dekker, "Electrical generation and absorption of phonons in carbon nanotubes," Nature **432**, 371 (2004).

[6] E. M. Weig, R. H. Blick, T. Brandes, J. Kirschbaum, W. Wegscheider, M. Bichler, and J. P. Kotthaus, "Single-electron-phonon interaction in a suspended quantum dot phonon cavity," Phys. Rev. Lett. **92**, 046804 (2004).

[7] J. Koch and F. von Oppen, "Franck-Condon blockade and giant Fano factors in transport through single molecules," Phys. Rev. Lett. **94**, 206804 (2005).

[8] W. Izumida and M. Grifoni, "Phonon-assisted tunnelling in interacting suspended single-wall carbon nanotubes," New Journal of Physics **7**, 244 (2005).

[9] S. Sapmaz, P. Jarillo-Herrero, Ya. M. Blanter, C. Dekker, and H. S. J. van der Zant, "Tunneling in suspended carbon nanotubes assisted by longitudinal phonons," Phys. Rev. Lett. **96**, 026801 (2006).

[10] J. Koch, F. von Oppen, and A. V. Andreev, "Theory of the Franck-Condon blockade regime," Phys. Rev. B **74**, 205438 (2006).

[11] E. A. Osorio, K. O'Neill, N. Stuhr-Hansen, O. F. Nielsen, T. Bjørnholm, and H. S. J. van der Zant, "Addition energies and vibrational fine structure measured in electromigrated single-molecule junctions based on an oligophenylenevinylene derivative," Advanced Materials **19**, 281 (2007).

[12] E. Burzurí, Y. Yamamoto, M. Warnock, X. Zhong, K. Park, A. Cornia, and H. S. J. van der Zant, "Franck-Condon blockade in a single-molecule transistor," Nano Letters **14**, 3191 (2014).

[13] A. K. Hüttel, M. Poot, B. Witkamp, and H. S. J. van der Zant, "Nanoelectromechanics of suspended carbon nanotubes," New Journal of Physics **10**, 095003 (2008).

[14] R. Leturcq, C. Stampfer, K. Inderbitzin, L. Durrer, C. Hierold, E. Mariani, M. G. Schultz, F. von Oppen, and K. Ensslin, "Franck-Condon blockade in suspended carbon nanotube quantum dots," Nature Physics **5**, 327 (2009).

[15] A. K. Hüttel, B. Witkamp, M. Leijnse, M. R. Wegewijs, and H. S. J. van der Zant, "Pumping of vibrational excitations in the Coulomb-blockade regime in a suspended carbon nanotube," Phys. Rev. Lett. **102**, 225501 (2009).

[16] J. O. Island, V. Tayari, A. C. McRae, and A. R. Champagne, "Few-hundred GHz carbon nanotube nanoelectromechanical systems (NEMS)," Nano Letters **12**, 4564 (2012).

[17] M. Ganzhorn, S. Klyatskaya, M. Ruben, and W. Wernsdorfer, "Strong spin–phonon coupling between a single-molecule magnet and a carbon nanotube nanoelectromechanical system," Nature Nanotechnology **8**, 165 (2013).

[18] M. Jung, J. Schindele, S. Nau, M. Weiss, A. Baumgartner, and C. Schnenberger, "Ultraclean single, double, and triple carbon nanotube quantum dots with recessed Re bottom gates," Nano Letters **13**, 4522 (2013).

[19] P. Weber, H. L. Calvo, J. Bohle, K. Goß, C. Meyer, M. R. Wegewijs, and C. Stampfer, "Switchable coupling of vibrations to two-electron carbon-nanotube quantum dot states," Nano Letters **15**, 4417 (2015).

[20] J. Cao, Q. Wang, and H. Dai, "Electron transport in very clean, as-grown suspended carbon nanotubes," Nature Materials **4**, 745 (2005).

[21] J. Park and P. L. McEuen, "Formation of a p-type quantum dot at the end of an n-type carbon nanotube," Applied Physics Letters **79**, 1363 (2001).

[22] G. A. Steele, G. Gotz, and L. P. Kouwenhoven, "Tunable few-electron double quantum dots and Klein tunnelling in ultraclean carbon nanotubes," Nature Nanotechnology **4**, 363 (2009).

[23] See the Supplemental Material at [url], which includes Refs. [4, 9, 10, 13–19, 38], for details on the harmonic side band energies, the evaluation of g, and for statistics on the electronic excited state behaviour.

[24] M. Marganska, D. R. Schmid, P. L. Stiller, A. Dirnaichner, Ch. Strunk, M. Grifoni, and A. K. Hüttel, "Shaping electron wave functions in a carbon nanotube with a parallel magnetic field," (2017), arXiv:1712.08545.

[25] M. Margańska *et al.*, (2018), in preparation.

[26] E. D. Minot, Y. Yaish, V. Sazonova, and P. L. McEuen, "Determination of electron orbital magnetic moments in carbon nanotubes," Nature **428**, 536 (2004).

[27] E. A. Laird, F. Kuemmeth, G. A. Steele, K. Grove-Rasmussen, J. Nygård, K. Flensberg, and L. P. Kouwenhoven, "Quantum transport in carbon nanotubes," Rev. Mod. Phys. **87**, 703 (2015).

[28] E. Mariani and F. von Oppen, "Electron-vibron coupling in suspended carbon nanotube quantum dots," Phys. Rev. B **80**, 155411 (2009).

[29] F. Cavaliere, E. Mariani, R. Leturcq, C. Stampfer, and M. Sassetti, "Asymmetric Franck-Condon factors in suspended carbon nanotube quantum dots," Phys. Rev. B **81**, 201303 (2010).

[30] A. Donarini, A. Yar, and M. Grifoni, "Spectrum and Franck-Condon factors of interacting suspended single-wall carbon nanotubes," New Journal of Physics **14**, 023045 (2012).

[31] D. R. Schmid, S. Smirnov, M. Marganska, A. Dirnaichner, P. L. Stiller, M. Grifoni, A. K. Hüttel, and C. Strunk, "Broken SU(4) symmetry in a Kondo-correlated carbon nanotube," Phys. Rev. B **91**, 155435 (2015).

[32] A. R. Akhmerov and C. W. J. Beenakker, "Boundary conditions for Dirac fermions on a terminated honeycomb lattice," Phys. Rev. B **77**, 085423 (2008).

[33] A. H. Castro Neto, F. Guinea, N. M. R. Peres, K. S. Novoselov, and A. K. Geim, "The electronic properties of graphene," Rev. Mod. Phys. **81**, 109 (2009).

[34] M. Marganska, M. del Valle, S. H. Jhang, C. Strunk, and M. Grifoni, "Localization induced by magnetic fields in carbon nanotubes," Phys. Rev. B **83**, 193407 (2011).

[35] C. Enss and S. Hunklinger, *Low-Temperature Physics* (Springer-Verlag, 2005).

[36] D. R. Schmid, P. L. Stiller, Ch. Strunk, and A. K. Hüttel, "Liquid-induced damping of mechanical feedback effects in single electron tunneling through a suspended carbon nanotube," Appl. Phys. Lett. **107**, 123110 (2015).

[37] S. Reinhardt, C. Butschkow, S. Geissler, A. Dirnaichner, F. Olbrich, C. Lane, D. Schröer, and A. K. Hüttel, "Lab::Measurement — a portable and extensible frame-

work for controlling lab equipment and conducting measurements," Computer Physics Communications **234**, 216 (2019).
[38] D. R. Schmid, P. L. Stiller, C. Strunk, and A. K. Hüttel, "Magnetic damping of a carbon nanotube nanoelectromechanical resonator," New Journal of Physics **14**, 083024 (2012).